Molecules and Cells

NSM00158 Specifically Disrupts the CtBP2-p300 Interaction to Reverse CtBP2-Mediated Transrepression and Prevent the Occurrence of Nonunion

Xun Chen[1,2,4], Wentao Zhang[2,4], Qian Zhang[3], Tao Song[2], Zirui Yu[2], Zhong Li[2], Ning Duan[2,*], and Xiaoqian Dang[1,*]

[1]Department of Orthopedics, The Second Affiliated Hospital of Xi'an Jiaotong University, Xi'an 710005, China, [2]Department of Orthopaedics, Honghui Hospital, Xi'an Jiaotong University, Xi'an 710054, China, [3]The Department of Surgery Room, Xi'an Daxing Hospital, Xi'an 710016, China, [4]These authors contributed equally to this work.
*Correspondence: duanning07@stu.xjtu.edu.cn (ND); fbbycx@stu.xjtu.edu.cn (XD)
https://doi.org/10.14348/molcells.2020.0042
www.molcells.org

Carboxyl-terminal binding proteins (CtBPs) are transcription regulators that control gene expression in multiple cellular processes. Our recent findings indicated that overexpression of *CtBP2* caused the repression of multiple bone development and differentiation genes, resulting in atrophic nonunion. Therefore, disrupting the CtBP2-associated transcriptional complex with small molecules may be an effective strategy to prevent nonunion. In the present study, we developed an *in vitro* screening system in yeast cells to identify small molecules capable of disrupting the CtBP2-p300 interaction. Herein, we focus our studies on revealing the *in vitro* and *in vivo* effects of a small molecule NSM00158, which showed the strongest inhibition of the CtBP2-p300 interaction *in vitro*. Our results indicated that NSM00158 could specifically disrupt CtBP2 function and cause the disassociation of the CtBP2-p300-Runx2 complex. The impairment of this complex led to failed binding of Runx2 to its downstream targets, causing their upregulation. Using a mouse fracture model, we evaluated the *in vivo* effect of NSM00158 on preventing nonunion. Consistent with the *in vitro* results, the NSM00158 treatment resulted in the upregulation of Runx2 downstream targets. Importantly, we found that the administration of NSM00158 could prevent the occurrence of nonunion. Our results suggest that NSM00158 represents a new potential compound to prevent the occurrence of nonunion by disrupting CtBP2 function and impairing the assembly of the CtBP2-p300-Runx2 transcriptional complex.

Keywords: atrophic nonunion, CtBP2, NSM00158, p300, Runx2

INTRODUCTION

The arrest of the bone fracture repair process often causes nonunion (Calori et al., 2017; Marsell and Einhorn, 2011). Various factors, such as inadequate fracture stabilization, poor blood supply, infection, and bone fracture positions, can lead to the pathophysiology of nonunion (Calori et al., 2017; Marsell and Einhorn, 2011). According to its radiological appearance, bone nonunion can be routinely classified into two groups—hypertrophic and atrophic nonunion (Calori et al., 2017; Marsell and Einhorn, 2011). Hypertrophic nonunion promotes effective healing with good blood flow to the frac-

Received 7 February, 2020; revised 12 April, 2020; accepted 22 April, 2020; published online 20 May, 2020

eISSN: 0219-1032

ture site (Morshed, 2014; Panteli et al., 2015). This type of fracture can heal, likely needing additional stability to form the union (Morshed, 2014; Panteli et al., 2015). An atrophic nonunion is characterized by lack sufficient blood supply to the ends of the fracture bones, which leads to the bone failing to mount a healing response (Morshed, 2014; Panteli et al., 2015). Clinically, the treatment of nonunion is mainly divided into two classes: surgical and nonsurgical treatment (Morshed, 2014; Panteli et al., 2015). For surgical treatment, patients have many options (e.g., bone graft and internal and external stabilization) according to their nonunion type (Kawamura and Chung, 2008; Lenza and Faloppa, 2015; Lenza et al., 2009). The most common nonsurgical treatment is the use of a bone stimulator, which delivers pulsed electromagnetic waves or ultrasonic waves at the fracture site to stimulate bone growth by increasing the expression of *BMPs* (bone morphogenetic proteins) and increasing osteoblast proliferation (Kawamura and Chung, 2008; Lenza and Faloppa, 2015; Lenza et al., 2009). Due to the complexity of nonunion cases, no medicine is available to specifically inhibit or attenuate the pathogenesis of nonunion (Kawamura and Chung, 2008; Lenza and Faloppa, 2015; Lenza et al., 2009). In recent years, great progress has been made in studying the underlying mechanisms of nonunion (Ding et al., 2018). The current evidence supports the idea that the pathogenesis of nonunion involves genetic factors, the inflammation status induced of pro-inflammatory cytokines, such as tumor necrosis factor-α (TNF-α) and interleukin-6 (IL-6), and the aberrant expression of multiple genes such as *BMPs*, *IGFs* (insulin-like growth factors), *MMPs* (matrix metalloproteinases), and *VEGF* (vascular endothelial growth factor) (Ding et al., 2018; Panteli et al., 2015). Moreover, disruption of some signaling pathways, such as the nitric oxide (NO) and the Wnt signaling pathway, can also cause nonunion (Ding et al., 2018; Panteli et al., 2015).

Most recently, an original study in our laboratory revealed that various bone development genes were downregulated by a transcriptional complex during the pathogenesis of atrophic nonunion (Zhang et al., 2018). Our results indicated that carboxyl-terminal binding protein 2 (CtBP2), an NADH-sensitive transcriptional corepressor, formed a complex with the histone acetyltransferase p300 and Runt-related transcription factor 2 (Runx2) (Zhang et al., 2018). The development of atrophic nonunion led to a low level of NADH, which inhibited CtBP2 dimerization, and the CtBP2 monomer associated with the p300-Runx2 complex (Zhang et al., 2018). The inhibitory role of CtBP2 prevented Runx2 from binding to the promoters of multiple bone-related genes, such as *OSC* (Osteocalcin), *ALPL* (alkaline phosphatase, biomineralization associated), *COL1A1* (Collagen 1A1), *IBSP* (integrin binding sialoprotein), *SPP1* (secreted phosphoprotein 1), and *MMP13* (Zhang et al., 2018). Our results revealed a fundamental transcriptional mechanism associated with the pathogenesis of atrophic nonunion, in which CtBP2 functions as a corepressor inhibiting the expression of Runx2 downstream targets (Zhang et al., 2018). In addition to CtBP2, its paralog CtBP1 has also been found to repress the expression of numerous genes involved in developmental and oncogenic processes (Blevins et al., 2017; Chinnadurai, 2003). Similar to CtBP2 activity, CtBP1 interacts with histone-modification enzymes such as histone acetyltransferases and histone deacetylases through a conserved PXDLS (X represents any amino acid) motif, which also associates with DNA-binding transcriptional factors to mediate gene transcription (Kim et al., 2005; Zhang et al., 2000). Based on the conserved mechanism by which CtBPs interact with their binding partners through the PXDLS motif, a CPP-E1A peptide has been developed to directly disrupt the interaction between CtBPs and their partners, which has been proven to reverse oncogenic phenotypes *in vitro* and *in vivo* (Blevins et al., 2018). The cyclic nonapeptide CP61 can disrupt CtBP dimerization and selectively inhibit the interaction of CtBP1 and NADH, thereby affecting CtBP-mediated transcription by restricting its ability to colocalize into the nucleus (Birts et al., 2013). Additionally, several small molecules have been discovered that reverse CtBP-mediated transcription repression (Birts et al., 2013; Blevins et al., 2015; Straza et al., 2010). For example, 4-methylthio-2-oxobutanoic acid (MTOB), the penultimate compound in the methionine-salvage pathway, removes CtBP2 from *BIK* (BCL2 interacting killer) promoter and causes the upregulation of *BIK* in colorectal cancer cells (Straza et al., 2010). NSC95397, 2,3-Bis[2-hydroxyethyl)thio]-1,4-naphthoquinone, functions as a weak substrate of CtBP dehydrogenase (Blevins et al., 2015). NSC95397 can specifically perturb CtBP-protein partner interactions, thereby reversing CtBP-mediated transcriptional repression (Blevins et al., 2015).

Our recent publication successfully established an *in vitro* high-throughput screening (HTS) method used in yeast cells to obtain small molecules that disrupt the interaction between TRADD (tumor necrosis factor receptor type 1-associated DEATH domain protein) and TRAF2 (TNF receptor-associated factor 2) (Wen et al., 2018). Using the same strategy in this study, we screened small molecules that disrupt the CtBP2-p300 interaction. We successfully discovered 13 small molecules that disrupted the CtBP2-p300 interaction, and we focused our current study only on revealing the underlying molecular mechanism of NSM00158, which showed the strongest inhibition of the CtBP2-p300 interaction among the compounds assessed in our preliminary results.

MATERIALS AND METHODS

Small-molecule screening

Small-molecule screening was performed following a previously described protocol (Wen et al., 2018). Briefly, we constructed pGADT7-CtBP2 and pGBKT7-p300 plasmids and cotransformed them into wild-type yeast cells (AH109). The transformed cells were selected on synthetic complete medium lacking Trp and Leu (SC-TL). The positive yeast colonies coexpressing CtBP2 and p300 were subjected to cell growth determination in synthetic complete medium lacking His, Trp and Leu (SC-HTL). One positive colony that could grow in the SC-HTL medium was chosen and grown to the mid-log phase (OD_{600} = 1.0) at 28°C for 24 h. After diluting the cells 10-fold to an OD_{600} = 0.1, an equal number of cells (49 μl) were added to 96-well plates and supplemented with 1.0 μl small molecules added to each well at the same concentration. The cells were then grown in an incubator at 28°C for

18 h. The optical density (OD) of the cells was determined at 600 nm using a Synergy HTX Multi-mode Reader (BioTek, USA). The candidate small molecules were chosen based on a standard of $OD_{600} < 0.2$ and were subjected to a second round of screening under identical growth condition to verify the reproducibility of the growth inhibition.

Cells and cell culture

Three primary osteoblast cell lines from healthy controls (HOB1, HOB2, and HOB3) and three primary osteoblast cell lines from atrophic nonunion samples (AOB1, AOB2, and AOB3) were isolated as described previously (Zhang et al., 2018). The cells were grown in Dulbecco's modified Eagle's medium (DMEM) (Cat. #12491015; Thermo Fisher Scientific, USA) supplemented with 10% fetal bovine serum (FBS, Cat. #F2442; Sigma-Aldrich, USA) and 1% penicillin-streptomycin (Cat. #15070063; Thermo Fisher Scientific) at 37°C with 5% CO_2.

Cell treatments with compounds

Cells were seeded in 6-well plates at a density of 1×10^6 per well and incubated overnight at 37°C. The cells were then washed twice with phosphate-buffered saline (PBS) buffer, followed by supplementation with fresh medium containing different concentrations of NSC95397 (0, 0.5, 2.5, 10, and 20 μM) (Cat. #N1786; Sigma-Aldrich), different concentrations of MTOB (0, 0.5, 1, 2, and 5 mM) (Cat. #561414; MedKoo Biosciences, USA), or different concentrations of NSM00158 (0, 0.4, 1, 2, and 4 μM) at 37°C for 18 h. After treatment, the cells were washed twice with PBS buffer, and protein lysis buffer or RNA lysis buffer was added to the cells to extract protein or total RNA, respectively.

RNA isolation and quantitative real-time polymerase chain reaction (qRT-PCR)

Total RNA was isolated using the RNeasy Mini Kit (Cat. #74104; Qiagen, USA) following the manufacturer's instructions. A total of 1.0 μg of RNA for each sample was used for reverse transcription using the ProtoScript First Strand cDNA synthesis kit (Cat. #E6300S; New England Biolabs, USA). After diluting 10-fold, the cDNAs were applied to measure gene expression levels using the SYBR Green Master Mix Kit (Cat. #1725271; Bio-Rad, USA) with the primers listed in Supplementary Table S1. The PCR procedures included 95°C for 3 min, followed by 40 cycles of 95°C for 30 s and 68°C for 30 s. The relative expression level of each gene was normalized to β-actin.

Western blot analysis

Cells and tissue samples were lysed in RIPA buffer (Cat. #89900; Thermo Fisher Scientific) supplemented with 1× protease inhibitor cocktail (Cat. #11697498001; Roche, USA). The cell lysates were resolved by 12% SDS-PAGE, and the proteins were transferred to polyvinylidene difluoride (PVDF) membranes and probed with primary and secondary antibodies, respectively. The following primary antibodies were used: anti-CtBP1 (Cat. #612042; BD Biosciences, USA), anti-CtBP2 (Cat. #612044; BD Biosciences), anti-OSC (Cat. #ab93876; Abcam, USA), anti-ALPL (Cat. #ab116592; Abcam), anti-COL1A1 (Cat. #PA1-26204; Thermo Fisher Scientific), anti-IBSP (Cat. #PA5-41327; Thermo Fisher Scientific), anti-SPP1 (Cat. #HPA027541; Sigma-Aldrich), anti-MMP13 (Cat. #ab39012; Abcam), anti-CUL4A (Cat. #ab92554; Abcam), anti-MAP2 (Cat. #ab5392; Abcam), anti-DCX (Cat. #AV41333; Sigma-Aldrich), anti-NSE (Cat. #SAB4300698; Sigma-Aldrich), and anti-GAPDH (Cat. #ab8254; Abcam). The secondary antibodies included anti-mouse IgG (Cat. #ab6728; Abcam) and anti-rabbit IgG (Cat. #ab6721; Abcam).

Protein binding by AlphaScreen assay

The coding sequences of CtBP1 and CtBP2 were cloned into a pGEX-6P-1 vector with *Bam*HI and *Eco*RI sites. The p300 truncation (1001-1091 amino acids) and E1A (adenovirus early region 1A) were cloned into a pGET28a-His vector with *Bam*HI and *Eco*RI sites. After sequencing to verify the successful constructs, the plasmids were transformed into BL21 competent cells. One positive colony for each transformation was grown to log phase and then induced by 1 mM isopropyl β-d-1-thiogalactopyranoside (IPTG) to produce the target proteins. The His-tagged and GST-fused proteins were purified using Ni-NTA Agarose (Cat. #30210; Qiagen) and glutathione Sepharose 4B resin (Cat. #GE17-0756-01; Sigma-Aldrich), respectively. The AlphaScreen assay was performed following a previous protocol (Blevins et al., 2015).

Competitive ELISA (enzyme-linked immunosorbent assay)

The competitive ELISAs were performed as described previously (Blevins et al., 2015). In brief, the 96-well plates were coated with CtBP2 in a buffer containing 50 mM Tris (pH 8.0) and 200 mM NaCl at room temperature for 2 h. After washing twice with PBS buffer, the plates were blocked with 1% BSA in a buffer containing 0.05% Tween-20, 50 mM Tris (pH 8.0), 250 mM NaCl, and 1 mM TCEP (Tris [2-carboxyethyl] phosphine) at room temperature for 2 h. The plates were then washed twice with PBS buffer, followed by incubation with GST-p300-R2 or GST-E1A in the presence of small molecules at room temperature for 1 h. After raising twice with PBS buffer, the plates were incubated with anti-GST antibody (#A7340; Sigma-Aldrich) at room temperature for 1 h. The plates were read in a Synergy HTX Multi-mode Reader.

Chromatin immunoprecipitation (ChIP)

The ChIP assay was carried out following a previously described protocol (Zhang et al., 2018). Briefly, AOB1, NSM00158-treated AOB1, HOB1, 2-DG (2-deoxy-D-glucose)-treated HOB1, NSM00158-treated HOB1, $CoCl_2$ (cobalt chloride)-treated HOB1, and NSM00158 + $CoCl_2$-treated HOB1 cells were washed twice with PBS buffer at room temperature for 5 min. The cells were then cross-linked in PBS buffer containing 1% formaldehyde for 15 min, and the reaction was stopped by adding 1 M glycine to a final concentration of 125 mM. After quenching for 5 min, the cells were washed twice with PBS buffer and then subjected to the ChIP procedure using a Millipore ChIP assay kit (Cat. #17295; Millipore, USA) according to the manufacturer's instructions. The antibodies used for ChIP included anti-CtBP1, anti-CtBP2, and anti-p300 (Cat. #sc-585; Santa Cruz Biotechnology, USA), anti-Runx2 (Cat. #sc-101145; Santa Cruz

Biotechnology), and mouse IgG (Cat. #sc-2025; Santa Cruz Biotechnology). The input and output DNA was used for the qRT-PCR analyses with the SYBR Green Master Mix kit using the primers listed in Supplementary Table S2.

Alkaline phosphatase (ALP) activity measurement

The ALP activity was determined using an ALP assay kit (Cat. #ab83369; Abcam) following the instructions provided by the manufacturer. Briefly, AOB3 cells (1×10^5) were treated with DMSO, 2 μM or 4 μM NSM00158 at 37°C for 18 h. After washing twice with PBS buffer, the cells were lysed in RIPA buffer and then centrifuged at 14,000 rpm at 4°C for 10 min. The protein concentrations in the supernatant were quantified by bicinchoninic acid assay. Then, equal volumes of cell lysate and substrate were mixed in a 96-well plate. After incubation at 37°C for 5 min, the reaction was terminated by stop buffer. The ALP activity was determined by measuring the absorbance at 405 nm.

Measurement of NADH/NAD$^+$ ratio

The NADH/NAD$^+$ ratio was measured using a colorimetric kit (Cat. #ab65348; Abcam). In brief, HOB1 cells were treated with 2 μM NSM00158, 1 mM 2-DG, 2-DG (1 mM) + NSM00158 (2 μM), 200 μM $CoCl_2$, or $CoCl_2$ (200 μM) + NSM00158 (2 μM) for 18 h. The treated cells were assayed to measure the NADH/NAD$^+$ ratio following the protocol provided by the manufacturer.

Alizarin red S staining and Von Kossa staining

AOB3 cells (1×10^4) were grown in osteogenic medium, which was composed of DMEM, 200 μM ascorbic acid, 100 nM dexamethasone, 10 mM β-glycerol-phosphate, and 2 μM (or 4 μM) NSM00158. The medium was replaced twice per week. After incubation for 14 days, the cells were washed twice with PBS buffer and then fixed with 2% paraformaldehyde for 20 min at 37°C. The cells were then stained with an alizarin red S staining solution (Cat. #TMS-008-C; Sigma-Aldrich) and a Von Kossa stain kit (Cat. #ab150687; Abcam) for 30 min at 37°C. After rinsing with ddH_2O five times, the stained cells were photographed.

Mouse fracture model and radiograph scoring assay

A total of 45 athymic nu/nu mice (male, 12 weeks of age, ~35 g body weight) from Shanghai SLAC Laboratory Animal Co. (China) underwent surgery in which femoral fractures were generated following a previous protocol (Oetgen et al., 2008). All fractures were immediately rodded, and the mice were randomly divided into three groups (n = 15 per group). The fractured bones were imaged using a Philips Digital Diagnost/Optimus 80 system. On the second day after surgery, the mice in the three groups were intraperitoneally injected (twice per week) with DMSO, 10 μM NSM00158, or 20 μM NSM00158. After 30 days, images were taken to evaluate the bone healing in each group. Calluses near the fractured bones were surgically taken from three representative mice in each group and the RNA and protein were isolated from them. The animal maintenance, surgery and treatments followed a protocol approved by the Institutional Animal Care and Use Committee (IACUC) of Xi'an Jiao Tong University (No. 20180910c), and all experimental procedures used in this study were performed in accordance with the approved guidelines of the ethical board of Xi'an Jiaotong University College of Medicine. The quantification of the bone healing after fracture was performed following a previous standard in which both the formation of callus and bone union were evaluated (Chen et al., 2013). For callus formation, the standard was 0 (no callus), 1 (mild, < 50%), 2 (moderate, > 50%), and 3 (full across the defect). For bone union, 0 (no union), 1 (mild, < 50%), 2 (moderate, > 50%), and 3 (full bone bridge). The images were blindly scored by three people, and then, the scores were calculated.

Statistical analysis

All experiments were independently replicated at least three times. The data are presented as the mean ± SD. Significance was determined by Student's *t*-test using the IBM SPSS Statistics (ver. 22; IBM, USA). In figures, $P < 0.05$, $P < 0.01$, and $P < 0.001$ are indicated by one asterisk (*), two asterisks (**), and three asterisks (***), respectively.

RESULTS

Identification of small molecules that specifically disrupt the CtBP2-p300 interaction in yeast cells

Our recent findings indicate that the CtBP2-p300-Runx2 transcriptional complex represses the expression of bone development genes in the pathogenesis of atrophic nonunion (Zhang et al., 2018). We speculated that blocking the CtBP2-p300 interaction might be an effective strategy to inhibit nonunion. To develop small molecules that specifically disrupt the CtBP2-p300 interaction, we performed an *in vitro* HTS with yeast cells using a small-molecule pool that harbors 20,000 chemical compounds derived from plants and marine species (Wen et al., 2018). Accordingly, we primarily constructed the yeast cell expression vectors pGADT7-CtBP2 and pGBKT7-p300. We then cotransformed different combinations of plasmids, including pGADT7-CtBP2 + pGBKT7-p300, pGADT7-CtBP2 + pGBKT7 and pGADT7 + pGBKT7-p300, into AH109 yeast cells. After selection in nutrient-deficient medium (SC-TL), the protein levels of CtBP2 and p300 in positive colonies were examined (Supplementary Fig. S1). Based on the principle of a yeast two-hybrid assay, we examined the interaction between CtBP2 and p300 using SC-HTL medium. The results showed that only cells expressing both CtBP2 and p300 could grow in the SC-HTL medium but not cells expressing CtBP2 or p300 alone (Fig. 1A). We also monitored cell growth at different time points (0, 4, 8, 12, 16, 20, and 24 h) in liquid SC-HTL medium, and these results also indicated that only cells expressing both CtBP2 and p300 could grow (Fig. 1B). Next, equal volumes of yeast cells co-expressing CtBP2 and p300 were seeded into 96-well plates, individual small molecules (4 μM) were added in each well. After incubating for 24 h, the cell density was examined, and the candidate compounds were assessed using a standard of $OD_{600} < 0.2$ (Fig. 1C). In total, we identified 13 small molecules that strongly inhibited the growth of the yeast cells, and their chemical structures are shown in Supplementary Fig. S2A. Among these 13 compounds, NSM00158 (Fig. 1D)

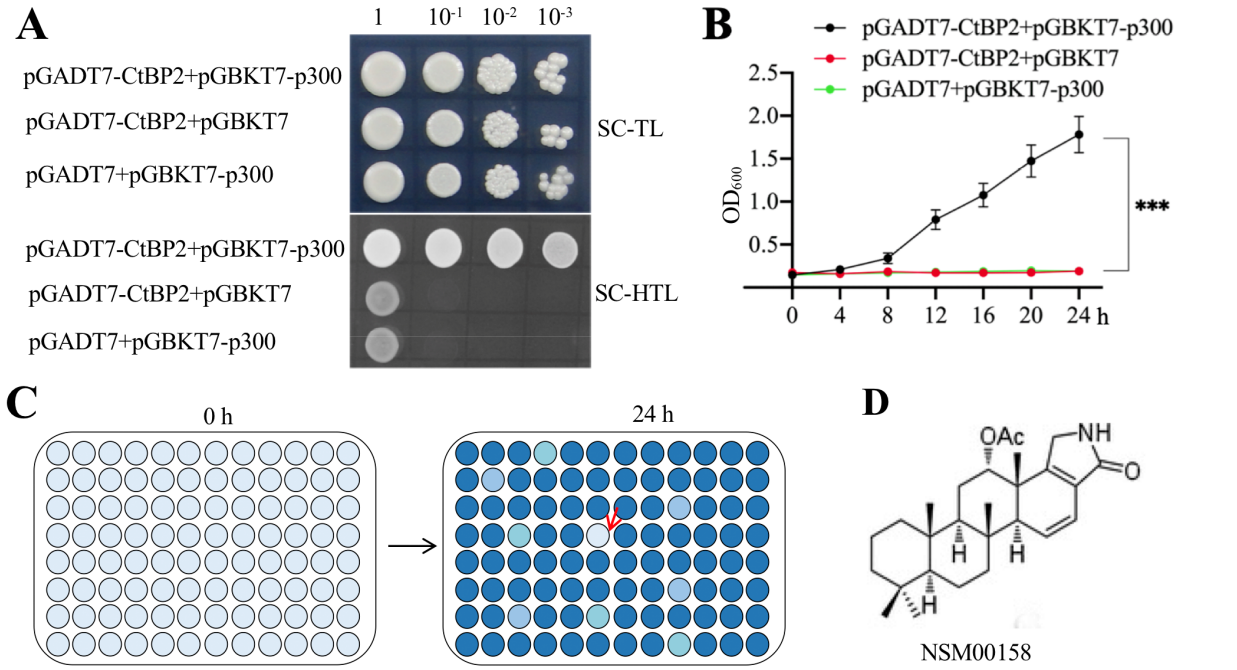

Fig. 1. Identification of small molecules that disrupted the CtBP2-p300 interaction in the yeast system. (A) CtBP2 interacted with p300 in yeast cells. Different combinations of plasmids were cotransformed into AH109 cells. The interaction between CtBP2 and p300 was determined in SC-TL medium (top panel) or SC-HTL medium (bottom panel). (B) Growth curve of yeast cells coexpressing CtBP2 and p300. Cells used in (A) were grown in SC-HTL medium for 0, 4, 8, 12, 16, 20, or 24 h, followed by OD_{600} measurement. ***P < 0.001. (C) Schematic representation of the small-molecule screening. AH109 yeast cells expressing *pGADT7-CtBP2* and *pGBKT7-p300* were grown in SC-HTL medium for 18 h at 30°C. Cells were diluted to OD_{600} = 0.1 using fresh SC-HTL medium and were seeded in equal concentrations in 96-well plates (left). After incubation at 30°C for 24 h (right), the cell density was measured using a Synergy HTX Multi-mode Reader. The red arrow represented an exampled well harboring a candidate compound. Small molecules that inhibited cell growth (OD_{600} < 0.2) were selected as candidates. (D) The chemical structure of NSM00158.

showed the strongest ability to inhibit the growth of cells co-expressing CtBP2 and p300 (Supplementary Fig. S2B).

NSM00158 functioned as an inhibitor of CtBP2 but not p300

To dissect how NSM00158 functions, we evaluated its effects on the interactions of CtBP2-p300, CtBP2-E1A, p300-c-MYC and p300-c-JUN in yeast cells. The CtBP2-p300 interaction, and the interactions of CtBP2-E1A, p300-c-MYC and p300-c-JUN were previously reported in other publications (Faiola et al., 2005; Lee et al., 1996; Zhao et al., 2008). Accordingly, we cotransformed different combinations of plasmids, including pGADT7-CtBP2 + pGBKT7-p300, pGADT7-CtBP2 + pGBKT7-E1A-Flag, pGADT7-c-MYC + pGBKT7-p300, and pGADT7-c-JUN + pGBKT7-p300, into AH109 yeast cells. After determining the protein levels in positive colonies (Supplementary Fig. S3A), we examined and verified protein interactions in the SC-HTL medium (Supplementary Fig. S3B, top panel). We next evaluated the effects of NSM00158 on these interactions. As shown in Supplementary Fig. S3B (bottom panel), supplementation with 4 μM NSM00158 inhibited the growth of the cells coexpressing pGADT7-CtBP2 + pGBKT7-p300 or pGADT7-CtBP2 + pGBKT7-E1A-Flag but did not affect the cells coexpressing pGADT7-c-MYC + pGBKT7-p300 or pGADT7-c-JUN + pGBKT7-p300. In addition, we also observed similar growth patterns of these cells at different time points (0, 4, 8, 12, 16, 20, and 24 h) in liquid SC-HTL medium supplemented with or without 4 μM NSM00158 (Supplementary Figs. S3C and S3D). These results suggested that NSM00158 functioned as an inhibitor of CtBP2 but not p300 because it only disrupted the interactions of CtBP2-p300 and CtBP2-E1A but not p300-c-MYC or p300-c-JUN.

We next aimed to determine the inhibitory efficiency of NSM00158. For this purpose, we primarily divided p300 into three regions: R1 (1-1000 amino acids), R2 (1001-1191 amino acids), and R3 (1192-2414 amino acids) (Supplementary Fig. S4A). The R2 region contained the PMDLS motif, which was proposed to be the binding site of CtBP2. To investigate whether CtBP2 only interacted with p300-R2, we transformed different combinations of plasmids, including pGADT7-CtBP2 + pGBKT7-p300, pGADT7-CtBP2 + pGBKT7-p300$^{\triangle PMDLS}$ (PMDLS motif-deleted mutant), pGADT7-CtBP2 + pGBKT7-p300-R1, pGADT7-CtBP2 + pGBKT7-p300-R2, and pGADT7-CtBP2 + pGBKT7-p300-R3, into AH109 yeast cells. As shown in Supplementary Figs. S4B and S4C, we observed that CtBP2 interacted only with p300-R2 but not with R1, R3 or p300$^{\triangle PMDLS}$. We purified the His-CtBP2 and GST-p300-R2 proteins (Supplementary Fig. S4D) and then performed the AlphaScreen binding reaction to determine their binding efficiency. We observed that the

protein binding signals increased with protein concentration (Supplementary Fig. S4E). Using plates-coated with 100 μM His-CtBP2, we added a mixture containing 150 μM GST-p300-R2 and different concentrations of NSM00158 into plates to perform a competitive ELISA. After washing the unbound GST-p300-R2, the remaining GST-p300-R2 was examined with a anti-GST antibody. The ELISA results indicated that NSM00158 could disrupt the CtBP2-p300-R2 interaction with a half maximal inhibitory concentration (IC_{50}) value of 1.71 ± 0.09 μM (Supplementary Fig. S4F).

As previously mentioned, NSC95397 and MTOB have been reported to inhibit CtBP1 and CtBP2 functions, respectively (Faiola et al., 2005; Lee et al., 1996; Zhao et al., 2008). Although NSC95397 has only been reported to disrupt CtBP1 function, we speculate that it could also inhibit CtBP2 because these two proteins share over 80% amino acid sequence identity and have similar functional domains (Supplementary Fig. S5A). To verify this possibility, we purified His-CtBP1, His-CtBP2, and GST-E1A (Supplementary Fig. S5B) and then performed competitive ELISAs to determine the effectiveness of NSC95397 to disrupt the CtBP1-E1A and CtBP2-E1A interactions. The ELISA results indicated that NSC95397 could disrupt the CtBP1-E1A and CtBP2-E1A interactions with IC_{50} values of 11.5 ± 0.98 μM and 10.34 ± 0.88 μM, respectively (Supplementary Figs. S5C and S5D). The similar IC_{50} values suggest that NSC95397 can also disrupt the CtBP2-E1A interaction. Thus, we next compared the inhibitory effects of NSM00158, NSC95397 and MTOB on the growth of yeast cells coexpressing CtBP2 and p300. Our results indicated that NSM00158 inhibited yeast cell growth with an IC_{50} value of 1.94 ± 0.08 μM, while NSC95397 and MTOB repressed cell growth with IC_{50} values of 10.2 ± 0.63 μM and 6.7 ± 0.44 mM, respectively (Supplementary Figs. S6A-S6C). To determine the specificity of NSM00158 in the inhibition of CtBP2-p300 and to compare the cell growth inhibitory abilities of different small molecules at the same concentration, we grew yeast cells with DMSO, 2 μM NSM00001 (a negative control, which was derived from the same small-molecule pool as NSM00158) (Supplementary Fig. S6D), NSM00158, NSC95397 and MTOB. Both the plate dotting and time point assays showed that NSM00158 exhibited the strongest inhibit effect on yeast cell growth, followed by NSC95397 and MTOB (Supplementary Figs. S6E and S6F). The negative control NSM00001 and DMSO did not inhibit yeast cell growth (Supplementary Figs. S6E and S6F). These results clearly suggested that NSM00158 was an inhibitor of CtBP2 and that it disrupted the interaction between CtBP2 and p300, thereby inhibiting yeast cell growth *in vitro*.

Given that CtBP1 and CtBP2 share a high identity of amino acid sequences and our results in Supplementary Fig. S5 showing that NSC95397 functions as an inhibitor of both CtBP1 and CtBP2, we speculated that NSM00158 would also block both CtBP1 and CtBP2. To verify this hypothesis, we grew cells coexpressing CtBP1/E1A-Flag or CtBP2/E1A-Flag in SC-HTL medium supplemented with or without NSM00158. The results showed that NSM00158 repressed the growth of cells coexpressing CtBP1/E1A-Flag or CtBP2/E1A-Flag (Supplementary Figs. S7A and S7B). In addition, the growth inhibition assay results indicated that NSM00158 repressed the growth of the cells coexpressing CtBP1/E1A-Flag or CtBP2/E1A-Flag with a similar IC_{50} value (Supplementary Figs. S7C and S7D). These results suggested that NSM00158 functioned as an inhibitor of both CtBP1 and CtBP2, in a manner similar to NSC95397.

Previous results have shown that NSC95397 is a weak substrate of CtBP1, and MTOB is also a substrate of CtBPs. To examine whether NSM00158 was a substrate of CtBP2, we performed an enzymatic assay to determine the NADH levels at increasing concentrations of NSM00158 by measuring absorption at the characteristic 340 nm wavelength. We also used the same concentrations of NSC95397 and MTOB as controls. Our results indicated that NSM00158 was a much weaker substrate than NSM00158 or MTOB (Supplementary Fig. S8), which suggested that NSM00158 might inhibit CtBP2 through a different functional mechanism than that of either NSC95937 or MTOB.

NSM00158 had no obvious cytotoxicity to inhibit human cell growth

One key question for the usage of NSM00158 in mammalian cells was its cytotoxicity because the optimal medication for the treatment of nonunion would convert AOB cells to HOB cells rather than killing them or inhibiting their growth. To evaluate whether NSM00158 induced cytotoxicity to inhibit cell proliferation, we isolated primary HOB and AOB cells and treated them with different concentrations of NSM00158 (0, 0.4, 1.0, 2.0, and 4.0 μM), NSC95397 (0, 0.5, 2.5, 10, and 20 μM), or MTOB (0, 1, 2, 5, and 10 mM). As shown in Supplementary Fig. S9, we did not observe significant growth inhibition in cells treated with different small molecules compared to untreated cells, which suggested that NSM00158 might be used for the treatment of nonunion.

NSM00158 treatment significantly induced the expression of the Runx2 target genes

Overexpression of CtBP2s inhibit the expression of multiple Runx2 target genes involved in bone formation and differentiation, including *OSC*, *ALPL*, *SPP1*, *COL1A1*, *IBSP*, and *MMP13* (Zhang et al., 2018). These genes were significantly downregulated in the AOB cells compared with those in the HOB cells (Zhang et al., 2018). Here, we also measured the protein levels of these genes, as well as CtBP1, CtBP2, p300, and CUL4A (used as a control), in three HOB and three AOB cell lines. Consistent with their mRNA levels, the protein levels of OSC, ALPL, SPP1, COL1A1, IBSP, and MMP13 were dramatically downregulated, while those of CtBP2 and p300 were significantly upregulated in the AOB cells (Fig. 2A, Supplementary Fig. S10A). Neither the CtBP1 nor CUL4A levels were obviously changed (Fig. 2A, Supplementary Fig. S10A). Next, we treated HOB1 and AOB3 cells with NSM00158 to evaluate whether it could affect the expression of CtBP2-p300-Runx2 targets. As expected, the NSM00158 treatment significantly induced the mRNA and protein levels of *OSC*, *ALPL*, *SPP1*, *COL1A1*, *IBSP*, and *MMP13* but not those of *CtBP1*, *CtBP2*, *p300*, and *CUL4A* (Figs. 2B-2D, Supplementary Fig. S10B). These results demonstrated that NSM00158 treatment abolished CtBP2-mediated transrepression. Moreover, we also performed alizarin red S staining and Von Kossa

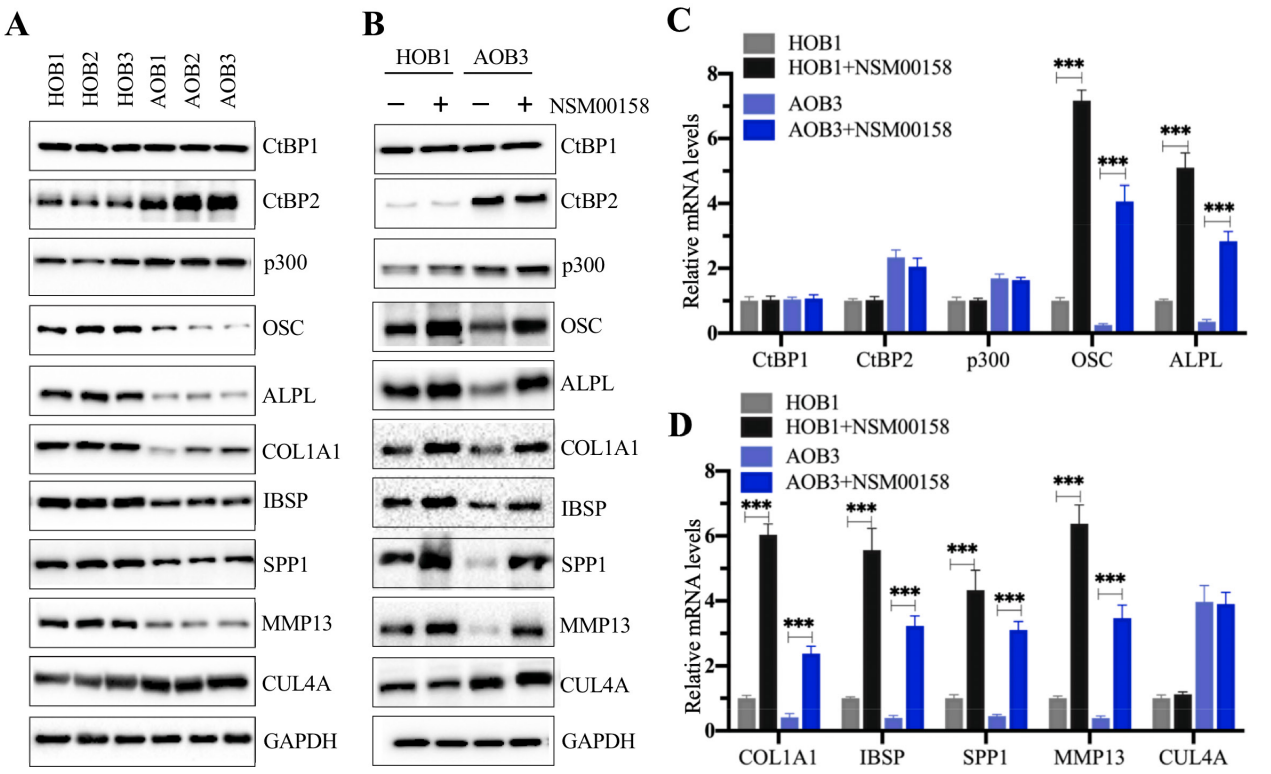

Fig. 2. NSM00158 significantly induced the expression of bone formation and differentiation genes. (A) The protein levels of bone formation and differentiation genes were significantly decreased in the AOB cells. Proteins were isolated from three HOB cell lines, HOB1, HOB2, and HOB3, and three AOB cell lines, AOB1, AOB2, and AOB3, and the protein levels of CtBP1, CtBP2, OSC, ALPL, COLA1, IBSP, SPP1, MMP13, and CUL4A were measured. GAPDH was used as a loading control. (B-D) NSM00158 significantly upregulated the expression of bone formation and differentiation genes. HOB1 and AOB3 cells were treated with or without 2.0 μM NSM00158 for 18 h, and then, measurements of the protein levels (B) and mRNA levels (C and D) of CtBP1, CtBP2, OSC, ALPL, COLA1, IBSP, SPP1, MMP13, and CUL4A were taken. $***P < 0.001$.

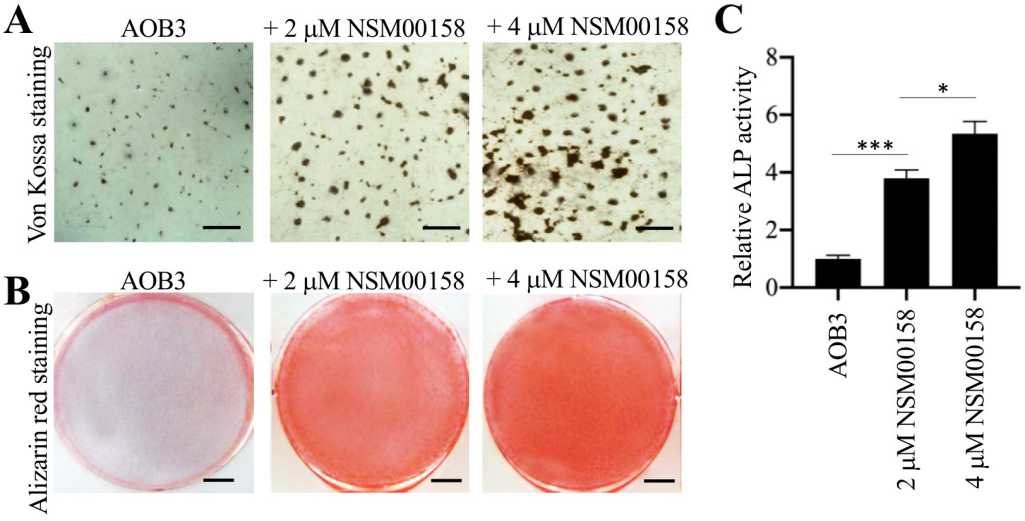

Fig. 3. NSM00158 significantly increased the mineralization and ALP activity of the cells. (A and B) Effect of NSM00158 on the mineralization in the AOB3 cells. AOB3 cells were grown in osteogenic medium for 14 days, followed by staining with Von Kossa (A) (scale bars = 1 mm) and alizarin red S (B) (scale bars = 1 cm). (C) Effect of NSM00158 on ALP activity in the AOB3 cells. AOB3 cells were grown in DMEM and then lysed in RIPA buffer. Equal volumes of cell lysate and substrate were mixed in a 96-well plate. After incubation at 37°C for 5 min, the reaction was terminated by supplementation with a stop buffer. The ALP activity was determined by measuring the absorbance at 405 nm. $*P < 0.05$, $***P < 0.001$.

staining to evaluate the effects of NSM00158 on osteoblastic differentiation and mineralization. As shown in Figs. 3A and 3B, our results showed that NSM00158 treatments (both 2 μM and 4 μM) significantly increased osteoblastic differentiation and mineralization. In addition, we also measured ALP activity after NSM00158 treatment. The results also indicated that NSM00158 markedly increased ALP activity (Fig. 3C). Additionally, we compared the effects of NSM00158 (2 μM), NSC95397 (10 μM), and MTOB (5 mM) on the expression levels of *OSC*, *ALPL*, *SPP1*, *COL1A1*, *IBSP*, and *MMP13* in the HOB1 and AOB1 cells. The results indicated that these three small molecules could significantly induce the mRNA and protein levels of the CtBP2-p300-Runx2 targets (Supplementary Figs. S11 and S12), which suggested that disruption of CtBP2 upregulated the expression of the Runx2 targets.

NSM00158 disrupted the binding of CtBP2 to the promoters of the Runx2 target genes

We next investigated the mechanism by which NSM00158 treatment increased the expression of the Runx2 target genes. We speculated that NSM00158 would decrease the occupancy of CtBP2 on the promoters of the Runx2 target genes, thereby inducing their expression. To verify this hypothesis, we treated AOB1 cells with or without NSM00158, and performed ChIP assays using anti-CtBP1, anti-CtBP2, anti-p300, anti-Runx2, or anti-IgG (negative control). Consis-

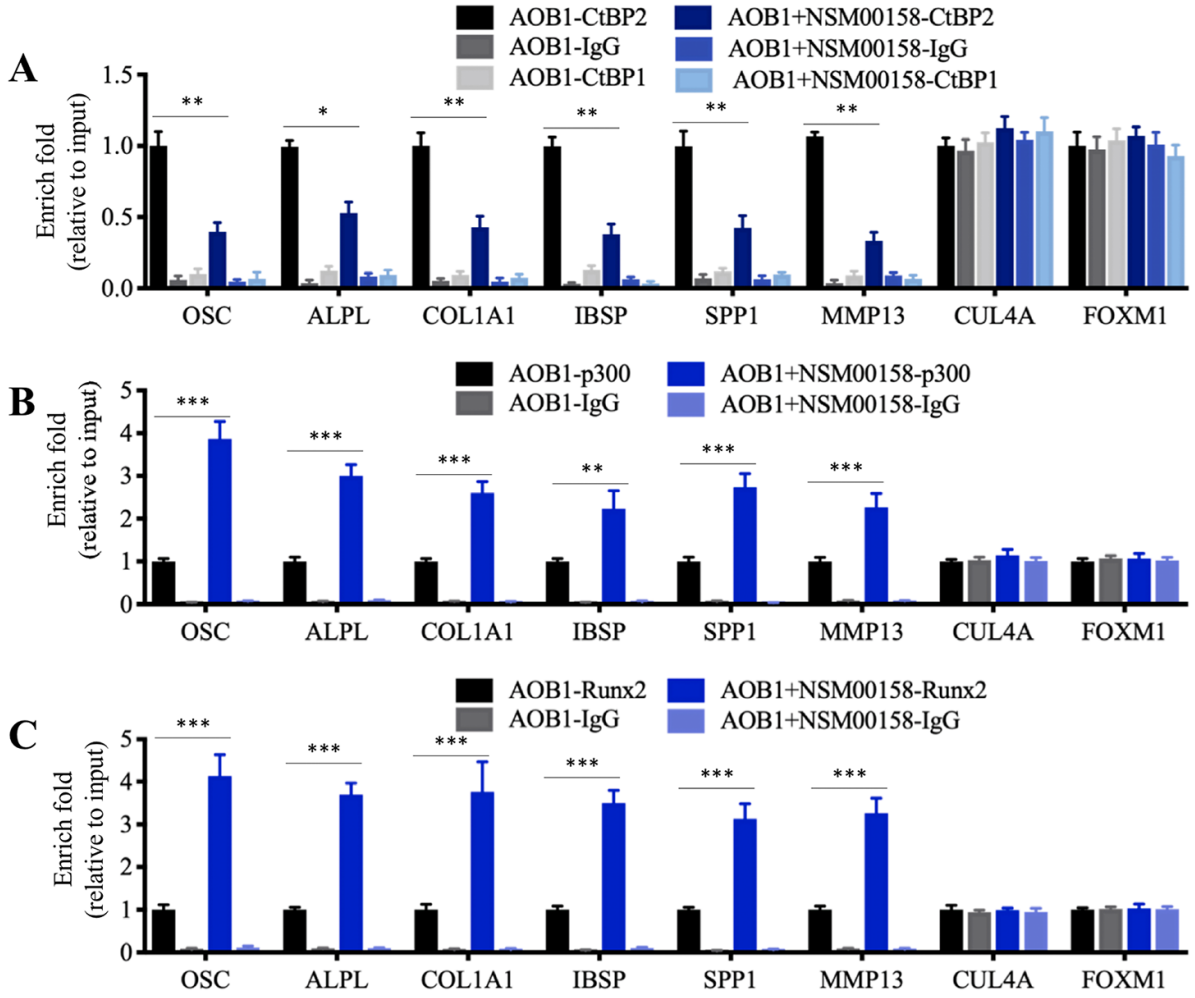

Fig. 4. NSM00158 significantly changed the occupancy of the CtBP2-p300-Runx2 complex at the promoters of the Runx2 target genes. (A) The occupancy of CtBP2 was significantly decreased at the promoters of the Runx2 target genes in the AOB1 cells. AOB1 cells were treated with or without 2.0 μM NSM00158 for 18 h and then subjected to ChIP assays using anti-CtBP1, anti-CtBP2, or IgG antibodies. qRT-PCR analyses were performed to evaluate their binding to the promoters of the Runx2 target genes. *CUL4A* and *FOXM1* were used as controls. $*P < 0.05$, $**P < 0.01$. (B) The occupancy of p300 at the promoters of the Runx2 target genes was significantly increased in the AOB1 cells. The cells described in Fig. 4A were subjected to ChIP assays using anti-p300 or IgG antibody, followed by qRT-PCR analyses to evaluate their binding to the promoters of the Runx2 target genes. *CUL4A* and *FOXM1* were used as controls. $**P < 0.01$, $***P < 0.001$. (C) The occupancy of Runx2 at the promoters of its target genes was significantly increased in the AOB1 cells. The cells described in Fig. 4A were subjected to ChIP assays using anti-Runx2 or IgG antibody, followed by qRT-PCR analyses to evaluate their binding to the promoters of the Runx2 target genes. *CUL4A* and *FOXM1* were used as controls. $***P < 0.001$.

tent with previous results (Zhang et al., 2018), CtBP2 but not CtBP1 bound to the promoters of *OSC*, *ALPL*, *SPP1*, *COL1A1*, *IBSP*, and *MMP13* without NSM00158 treatment (Fig. 4A). NSM00158 treatment significantly reduced the occupancy of CtBP2 on the promoters of these Runx2 target genes (Fig. 4A). In contrast, the occupancy levels of p300 and Runx2 were significantly increased after NSM00158 treatment compared to the occupancy level in the untreated cells (Figs. 4B and 4C). We did not find that NSM00158 treatment affected the enrichment of CtBP1, CtBP2, p300, and Runx2 at the promoters of CUL4A and FOXM1 (Fig. 4). These results verified the conclusion that CtBP2 acted as a repressor to inhibit p300-Runx2-mediated transcription, and NSM00158 reversed the repression of CtBP2, eventually causing the up-regulation of *OSC*, *ALPL*, *SPP1*, *COL1A1*, *IBSP*, and *MMP13*.

NSM00158 reversed the effect of the NADH decrease on the expression of the Runx2 target genes

Intracellular NAD^+ and NADH levels determine CtBP functions, especially affecting their binding to particular gene promoters (Fjeld et al., 2003). Our previous results showed that an elevated NADH level upregulated the expression of the Runx2 target genes by affecting the binding of the CtBP2-p300-Runx2 complex to their promoters (Zhang et al., 2018). The results presented above showed that NSM00158 affected the occupancy of CtBP2-p300-Runx2 at the promoters of the Runx2 target genes studied. To investigate the coeffects of NSM00158 and NDAH levels on the expression of the Runx2 targets, we treated HOB1 cells with both NSM00158 and 2-DG (a glycolytic inhibitor that reduces NADH levels) or with both NSM00158 and $CoCl_2$ (a chemical that increases NADH levels). After administering these treatments, we first measured the NADH/NAD^+ ratios. Our results indicated that 2-DG treatment alone significantly decreased the NADH/NAD^+ ratio (Supplementary Fig. S13). In contrast, treatment with $CoCl_2$ alone resulted in an increase in intracellular NADH levels (Supplementary Fig. S13). Treatment with NSM00158 alone did not change the intracellular NADH level (Supplementary Fig. S13). We also did not observe significant changes in the NADH/NAD^+ ratio in the cells treated with 2-DG (or $CoCl_2$) alone compared to that in the cells treated with NSM00158 + 2-DG (or NSM00158 + $CoCl_2$) (Supplementary Fig. S13). We next determined the expression of the Runx2 targets in these treated cells. The qRT-PCR results showed that 2-DG treatment alone dramatically decreased the expression levels of *OSC*, *ALPL*, *SPP1*, *COL1A1*, *IBSP*, and *MMP13* compared with those in the HOB1-untreated cells (Fig. 5A). In contrast, $CoCl_2$ treatment alone induced their expression (Fig. 5A). Interestingly, we identified that treatment with NSM00158 + 2-DG significantly induced the expression of the Runx2 targets compared with the HOB1-2DG-treated cells (Fig. 5A). The mRNA levels of the Runx2 targets were dramatically increased in the cells treated with NSM00158 + $CoCl_2$ compared with those in the cells treated with $CoCl_2$ alone

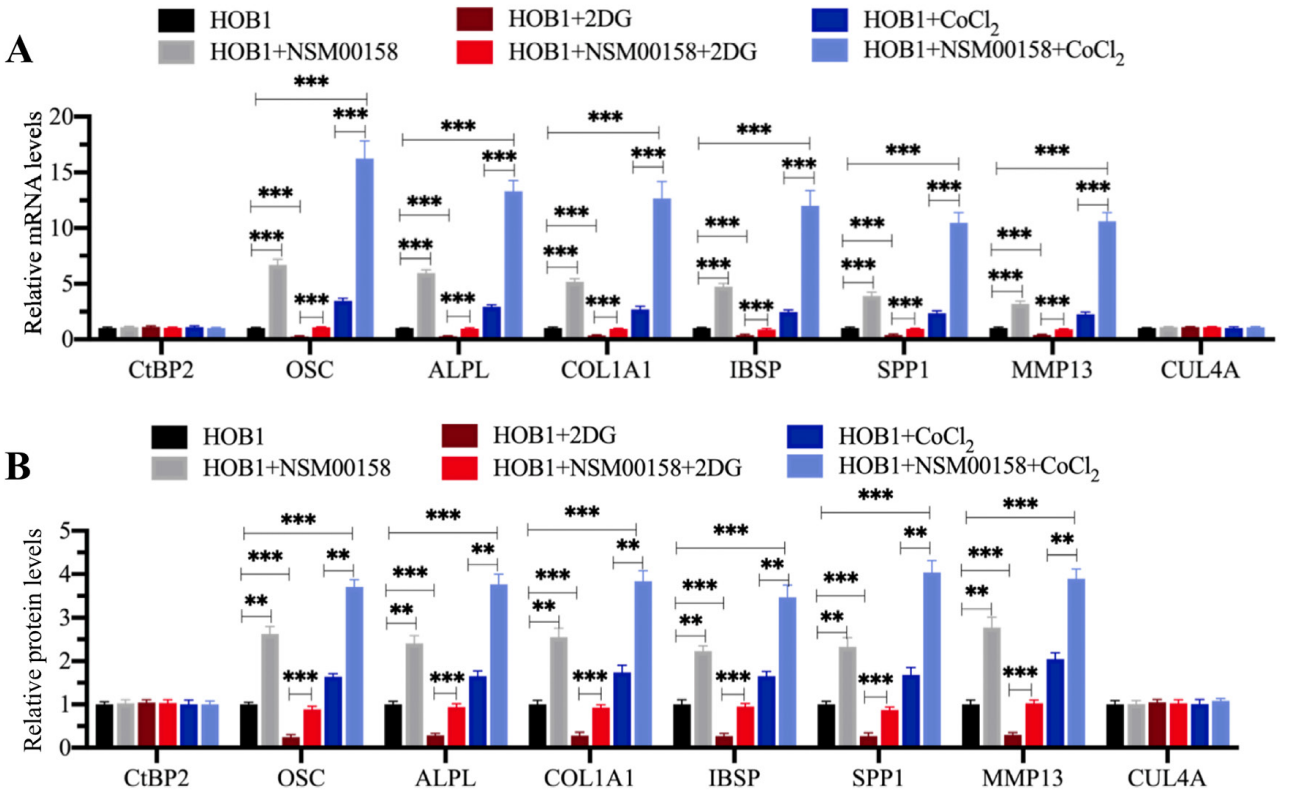

Fig. 5. NSM00158 treatment reversed the effect of the NADH decrease on CtBP2 expression. HOB1 cells were treated with 1 mM 2-DG, 2.0 μM NSM00158 + 1 mM 2-DG, 200 μm $CoCl_2$, or 2.0 μM NSM00158 + 200 μm $CoCl_2$ for 18 h, and then, the mRNA levels (A) and relative protein levels (B) of CtBP2, OSC, ALPL, COLA1, IBSP, SPP1, MMP13, and CUL4A were measured. $^{**}P < 0.01$, $^{***}P < 0.001$.

(Fig. 5A). Additionally, we examined the protein levels of these Runx2 targets after treatment with 2-DG, NSM00158 + 2-DG, $CoCl_2$ or NSM00158 + $CoCl_2$. Similar to those in their mRNA levels, we observed the same change patterns in the protein levels (Fig. 5B, Supplementary Fig. S14). These results suggested that NSM00158 reversed the effect of the NADH decrease on the expression of the Runx2 target genes.

To investigate the underlying mechanism of the expression changes of the Runx2 targets upon treatment with NSM00158 + 2-DG and NSM00158 + $CoCl_2$ compared with that of 2-DG or $CoCl_2$ alone, we performed ChIP assays using anti-CtBP2, anti-p300 and anti-Runx2. Our results indicated that 2-DG treatment significantly increased the occupancy of CtBP2 but dramatically decreased the occupancies of p300 and Runx2 at the promoters of *OSC*, *ALPL*, *SPP1*, *COL1A1*, *IBSP*, and *MMP13* (Fig. 6). NSM00158 + 2-DG treatment reversed this effect and caused a decrease in the CtBP2 occupancy but an increase in the p300 and Runx2 occupancies at the promoters of the Runx2 target genes (Fig. 6). On the other hand, $CoCl_2$ treatment dramatically decreased the occupancy of CtBP2 but significantly increased the occupancies of p300 and Runx2 at the promoters of *OSC*, *ALPL*, *SPP1*, *COL1A1*, *IBSP*, and *MMP13* (Fig. 6). Treatment with NSM00158 + $CoCl_2$ exacerbated this effect and caused much lower CtBP2 occupancy but higher p300 and Runx2 occupancies at the promoters of the Runx2 target genes compared with those upon $CoCl_2$ treatment alone (Fig. 6). These results revealed the mechanism by which NSM00158 disrupted

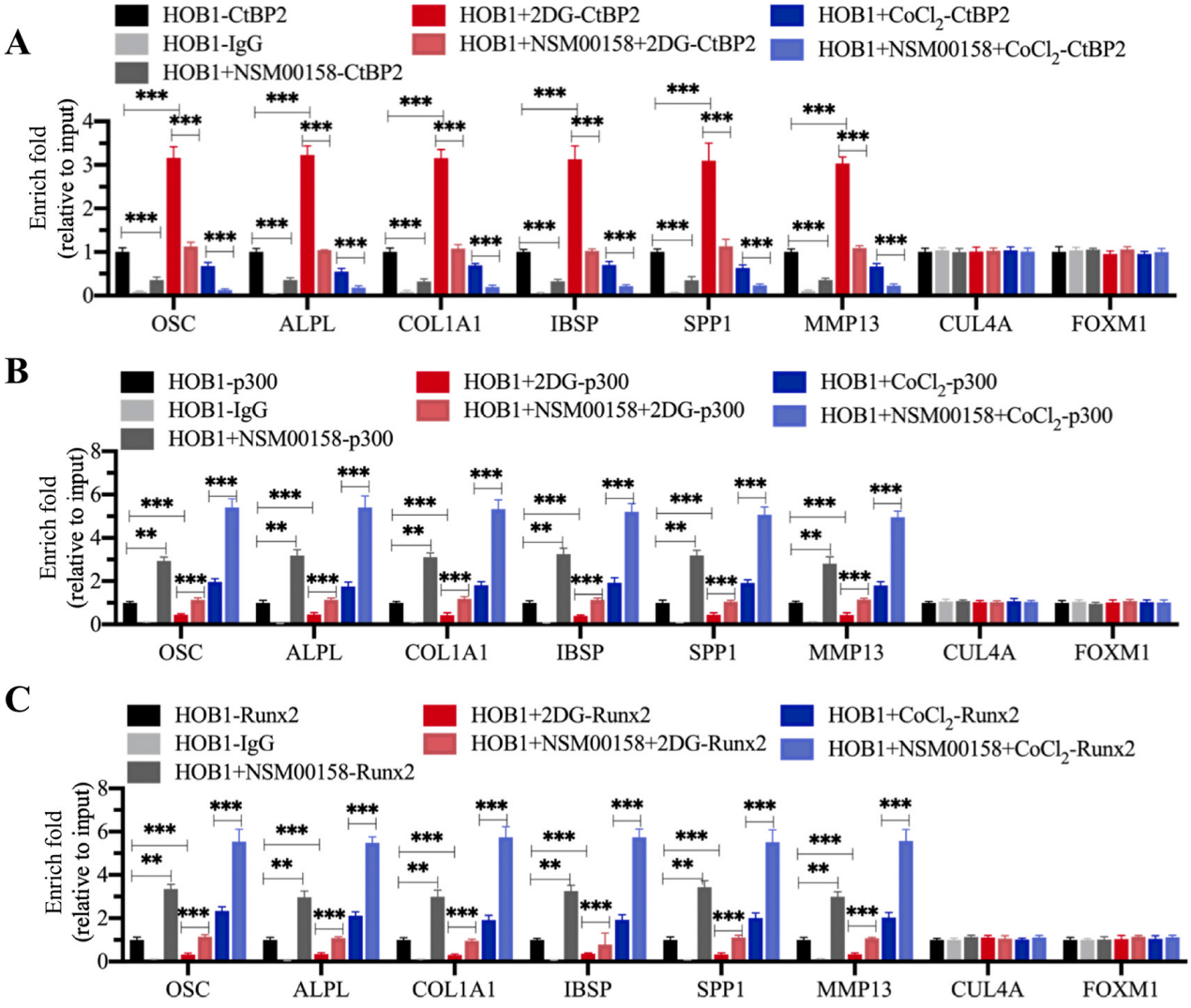

Fig. 6. NSM00158 treatment reversed the effect of the NADH decrease on the binding of the CtBP2-p300-Runx2 complex at the promoters of the Runx2 target genes. HOB1 cells were treated with 1 mM 2-DG, 2.0 μM NSM00158 + 1 mM 2-DG, 200 μm $CoCl_2$, and 2.0 μM NSM00158 + 200 μm $CoCl_2$ for 18 h. The cells were then subjected to ChIP assays using anti-CtBP2 (A), anti-p300 (B), or anti-Runx2 (C) antibodies. The IgG antibody was used as a negative control. qRT-PCR analyses were performed to evaluate their binding at the promoters of the Runx2 target genes, including *OSC*, *ALPL*, *COLA1*, *IBSP*, *SPP1*, and *MMP13*. *CUL4A* and *FOXM1* were used as controls. $^{**}P < 0.01$, $^{***}P < 0.001$.

the assembly of the CtBP2-p300-Runx2 complex and thus increased the occupancies of p300 and Runx2 at the promoters of their downstream targets. Importantly, the results showed that NSM00158 could reverse the effect caused by the NADH decrease, implying that NSM00158 can be used to increase the expression of +Runx2 target genes when nonunion occurs.

NSM00158 promoted fracture healing *in vivo*

Our results together with the results from our previous study showing that CtBP2 was overexpressed and repressed the expression of the Runx2 targets in the pathogenesis of nonunion (Zhang et al., 2018) encouraged us to determine the *in vivo* ability of NSM00158 to prevent the occurrence of nonunion. For this purpose, we established a mouse fracture model, with all fractures immediately rodded after surgery. A total of 45 mice with femoral fractures were randomly divided into three groups (n = 15 per group), and they were injected with DMSO, 10 μM NSM00158, or 20 μM NSM00158. Thirty days after the administration of NSM00158, we imaged the fractured bones and evaluated the extent of the healing. Our statistical data suggested that NSM00158 could significantly promote fracture healing *in vivo* (Supplementary Table S3). In the control group (DMSO), the fractures were healed in only 40% of mice (Supplementary Table S3), and the other 60% of the mice presented with nonunion (Fig. 7A, top panel). In contrast, after injection with 10 μM and 20 μM NSM00158, the percentage of healing mice was 73.3% and 86.7%, respectively (Supplementary Table S3; Fig. 7A, middle and bottom panels). Moreover, we quantified the radiographic scores of callus formation and bone union. The results also showed that the administration of NSM00158 significantly promoted callus formation and bone union (Figs. 7B and 7C). To determine the effect of NSM00158 on the Runx2 targets *in vivo*, we collected calluses from three mice in the control group presenting with nonunion and three healed mice in both the 10 μM and 20 μM NSM00158 groups, as determined after the mRNA and protein levels of the Runx2 tar-

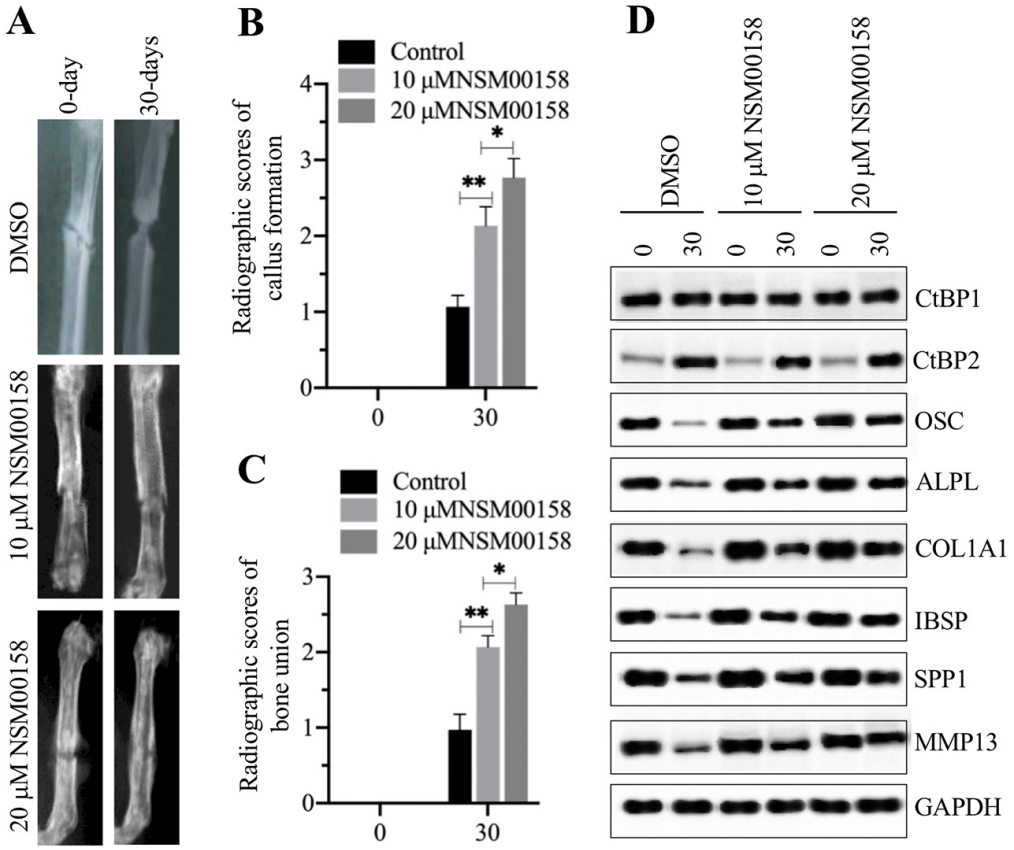

Fig. 7. NSM00158 prevented the occurrence of nonunion *in vivo*. (A) NSM00158 prevented the occurrence of nonunion *in vivo*. Femoral fractures were generated in 45 mice, which were randomly divided into three groups (n = 15 per group). On the second day after surgery, the mice in the three groups were injected with DMSO, 10 μM NSM00158, or 20 μM NSM00158. Bone fractures and the extent of their healing were determined using X-ray images taken 0 and 30 days after surgery. (B and C) Radiographic scores of the callus formation and bone union. The images of the fractured bones in the mice from the different groups described in Fig. 7A were quantified to determine the scores of callus formation (B) and bone union (C). $*P < 0.05$, $**P < 0.01$. (D) NSM00158 treatment increased the protein levels of the Runx2 targets *in vivo*. Calluses from three mice presenting with nonunion in the DMSO-injected group and three healed mice in both the 10 μM and 20 μM NSM00158 groups were collected, and total protein was isolated. Cell extracts were used to determine the protein levels of CtBP2, OSC, ALPL, COLA1, IBSP, SPP1, and MMP13. GAPDH was used as a loading control.

gets were determined. Our results indicated that NSM00158 treatment significantly increased the expression of the Runx2 targets *in vivo* (Fig. 7D, Supplementary Figs. S15 and S16).

DISCUSSION

CtBP-associated transcriptional complexes mediate the expression of multiple genes involved in development and oncogenesis (Chinnadurai, 2002; 2009; Ray et al., 2014). Recently, we identified that CtBP2, but not CtBP1, was overexpressed in atrophic nonunion tissues (Zhang et al., 2018). The molecular mechanism of this biological process revealed involved the CtBP2-p300-Runx2 complex specifically binding to the promoters of bone formation and differentiation genes, including *OSC*, *ALPL*, *SPP1*, *COL1A1*, *IBSP*, and *MMP13*, and repressed their expression (Zhang et al., 2018). Emerging evidence has suggested that the disruption of CtBP-mediated gene repression might be an effective strategy to treat diseases (Zhang et al., 2018). In the present study, we developed an *in vitro* screening method to identify small molecules that could specifically disrupt the CtBP2-p300 interaction. Using different strategies, we validated NSM00158 as an inhibitor of CtBP2. The *in vitro* and *in vivo* analyses suggested that treatment with NSM00158 could reverse CtBP2-mediated transrepression, causing the upregulation of *OSC*, *ALPL*, *SPP1*, *COL1A1*, *IBSP*, and *MMP13* and preventing the occurrence of nonunion (Fig. 8).

Different strategies, including two peptides (CP61 and CPP-E1A) and two small molecules (NSC95397 and MTOB), blocked CtBP function (Birts et al., 2013; Blevins et al., 2015; 2017; Straza et al., 2010). The CPP-E1A peptide inhibited CtBP1-mediated transrepression and reversed oncogenic phenotypes *in vitro* and *in vivo* by disrupting the interaction between CtBP and a transcription factor partner through the PXDLS motif (Blevins et al., 2015). Both NSC95397 and MTOB are substrates of CtBPs, and they can reverse CtBP-mediated transcription through different mechanisms (Birts et al., 2013; Blevins et al., 2015; 2017; Straza et al., 2010). NSC95397 is through to induce a conformational change in CtBP1, which may prevent CtBP1 from binding to transcription factors (Birts et al., 2013; Blevins et al., 2015; 2017; Straza et al., 2010). Structurally, CtBPs binds MTOB in the active-site clefts within their substrate-binding domains, while MTOB interact with catalytically conserved residues, thus blocking CtBP function (Birts et al., 2013; Blevins et al., 2015; 2017; Straza et al., 2010). Moreover, MTOB treatment can reduce the occupancies of CtBPs at the promoters of their targets (Birts et al., 2013; Blevins et al., 2015; 2017; Straza et al., 2010). In the current study, we revealed that NSM00158 was a specific inhibitor of CtBP2 but not of p300 (Supplementary Figs. S3 and S4). Compared to that of NSC95397 and MTOB, NSM00158 showed much weaker binding to CtBP2 (Supplementary Fig. S6). Importantly, we found that NSM00158 was a much weaker substrate than NSC95397 or MTOB (Supplementary Fig. S8). On the basis of these three important findings, together with the results showing that the NSM00158 treatment did not change intracellular NADH levels (Supplementary Fig. S13), we speculate that NSM00158 changes the conformational structure of CtBP2. We are currently investigating the CtBP2 conformational change with different doses of NSM00158 treatments, which may answer the question of how NSM00158 inhibits CtBP2 function and thus affects the transcription mediated by CtBP2.

The IC_{50} value of NSM00158 in inhibiting yeast cell growth was lower than that of either NSC95397 or MTOB, which indicates that NSM00158 is a stronger inhibitor of CtBP2 (Supplementary Fig. S6). Interestingly, NSM00158 did not show obvious cytotoxicity during its inhibition of HOB and AOB cell growth (Supplementary Fig. S9). These results, together with the promising *in vivo* result of the NSM00158 experiments in preventing nonunion occurrence, suggest that it may be a candidate compound for promoting fracture healing. CtBP1 and CtBP2 are highly homologous proteins, and we found that the CtBP1 inhibitor NSC95397 can also repress CtBP2 function. This result, together with our finding that NSM00158 can inhibit both CtBP1 and CtBP2 *in vitro*, suggests that NSM00158 can be used to reverse CtBP1-mediated transrepression in other biological processes, especially tumorigenesis.

In conclusion, we screened the compound NSM00158, which could specifically disrupt the CtBP2-p300 interaction,

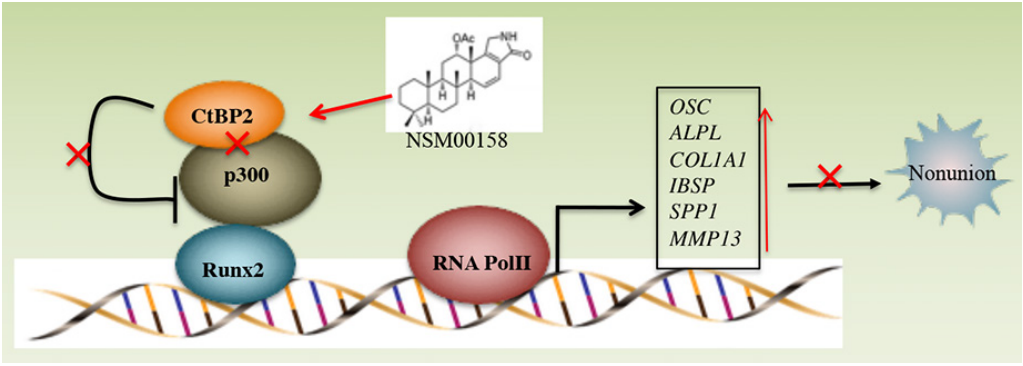

Fig. 8. A schematic of the NSM00158 mechanism preventing nonunion occurrence. The small-molecule compound NSM00158 specifically inhibited CtBP2 function and caused the disassociation of CtBP2 from the CtBP2-p300-Runx2 complex. The released p300-Runx2 complex binds to the promoters of bone development and differentiation genes, including *OSC*, *ALPL*, *COLA1*, *IBSP*, *SPP1*, and *MMP13,* to activate their expression. The induction of these genes prevented the occurrence of nonunion.

impair the binding of the CtBP2-p300-Runx2 complex at the promoters of bone formation and differentiation genes, and lead to their upregulation. The *in vivo* evaluation indicated that NSM00158 could prevent nonunion occurrence and promote fracture healing effectively. Our results may profoundly prevent nonunion occurrence and other diseases that are caused by aberrant gene expression mediated by CtBP2.

Note: Supplementary information is available on the Molecules and Cells website (www.molcells.org).

ACKNOWLEDGMENTS

This work was supported by two projects from the Key Science and Technology Program of Shaanxi Province, China (grant No. 2015SF110 and No. 2013K14-02-12).

AUTHOR CONTRIBUTIONS

X.D. and N.D. designed the experiments and wrote the manuscript. X.C. and W.Z. performed the experiments. Q.Z. and T.S. performed statistical analyses and helped animal maintenance. Z.Y. and Z.L. provided reagents, expertise and feedback.

CONFLICT OF INTEREST

The authors have no potential conflicts of interest to disclose.

ORCID

Xun Chen	https://orcid.org/0000-0003-1374-6154
Wentao Zhang	https://orcid.org/0000-0002-0546-6745
Qian Zhang	https://orcid.org/0000-0003-4703-1018
Tao Song	https://orcid.org/0000-0002-1700-8039
Zirui Yu	https://orcid.org/0000-0003-1509-7848
Zhong Li	https://orcid.org/0000-0001-6665-8321
Ning Duan	https://orcid.org/0000-0003-3974-4683
Xiaoqian Dang	https://orcid.org/0000-0002-3594-6627

REFERENCES

Birts, C.N., Nijjar, S.K., Mardle, C.A., Hoakwie, F., Duriez, P.J., Blaydes, J.P., and Tavassoli, A. (2013). A cyclic peptide inhibitor of C-terminal binding protein dimerization links metabolism with mitotic fidelity in breast cancer cells. Chem. Sci. *4*, 3046-3057.

Blevins, M.A., Huang, M., and Zhao, R. (2017). The role of CtBP1 in oncogenic processes and its potential as a therapeutic target. Mol. Cancer Ther. *16*, 981-990.

Blevins, M.A., Kouznetsova, J., Krueger, A.B., King, R., Griner, L.M., Hu, X., Southall, N., Marugan, J.J., Zhang, Q., Ferrer, M., et al. (2015). Small molecule, NSC95397, inhibits the CtBP1-protein partner interaction and CtBP1-mediated transcriptional repression. J. Biomol. Screen. *20*, 663-672.

Blevins, M.A., Zhang, C., Zhang, L., Li, H., Li, X., Norris, D.A., Huang, M., and Zhao, R. (2018). CPP-E1A fusion peptides inhibit CtBP-mediated transcriptional repression. Mol. Oncol. *12*, 1358-1373.

Calori, G.M., Mazza, E.L., Mazzola, S., Colombo, A., Giardina, F., Romano, F., and Colombo, M. (2017). Non-unions. Clin. Cases Miner. Bone Metab. *14*, 186-188.

Chen, L., Yang, X., Huang, G., Song, D., Ye, X.S., Xu, H., and Li, W. (2013). Platelet-rich plasma promotes healing of osteoporotic fractures. Orthopedics *36*, e687-e694.

Chinnadurai, G. (2002). CtBP, an unconventional transcriptional corepressor in development and oncogenesis. Mol. Cell *9*, 213-224.

Chinnadurai, G. (2003). CtBP family proteins: more than transcriptional corepressors. Bioessays *25*, 9-12.

Chinnadurai, G. (2009). The transcriptional corepressor CtBP: a foe of multiple tumor suppressors. Cancer Res. *69*, 731-734.

Ding, Z.C., Lin, Y.K., Gan, Y.K., and Tang, T.T. (2018). Molecular pathogenesis of fracture nonunion. J. Orthop. Translat. *14*, 45-56.

Faiola, F., Liu, X., Lo, S., Pan, S., Zhang, K., Lymar, E., Farina, A., and Martinez, E. (2005). Dual regulation of c-Myc by p300 via acetylation-dependent control of Myc protein turnover and coactivation of Myc-induced transcription. Mol. Cell. Biol. *25*, 10220-10234.

Fjeld, C.C., Birdsong, W.T., and Goodman, R.H. (2003). Differential binding of NAD+ and NADH allows the transcriptional corepressor carboxyl-terminal binding protein to serve as a metabolic sensor. Proc. Natl. Acad. Sci. U. S. A. *100*, 9202-9207.

Kawamura, K. and Chung, K.C. (2008). Treatment of scaphoid fractures and nonunions. J. Hand Surg. Am. *33*, 988-997.

Kim, J.H., Cho, E.J., Kim, S.T., and Youn, H.D. (2005). CtBP represses p300-mediated transcriptional activation by direct association with its bromodomain. Nat. Struct. Mol. Biol. *12*, 423-428.

Lee, J.S., See, R.H., Deng, T., and Shi, Y. (1996). Adenovirus E1A downregulates cJun- and JunB-mediated transcription by targeting their coactivator p300. Mol. Cell. Biol. *16*, 4312-4326.

Lenza, M., Belloti, J.C., Gomes Dos Santos, J.B., Matsumoto, M.H., and Faloppa, F. (2009). Surgical interventions for treating acute fractures or non-union of the middle third of the clavicle. Cochrane Database Syst. Rev. (4), CD007428.

Lenza, M. and Faloppa, F. (2015). Surgical interventions for treating acute fractures or non-union of the middle third of the clavicle. Cochrane Database Syst. Rev. (5), CD007428.

Marsell, R. and Einhorn, T.A. (2011). The biology of fracture healing. Injury *42*, 551-555.

Morshed, S. (2014). Current options for determining fracture union. Adv. Med. *2014*, 708574.

Oetgen, M.E., Merrell, G.A., Troiano, N.W., Horowitz, M.C., and Kacena, M.A. (2008). Development of a femoral non-union model in the mouse. Injury *39*, 1119-1126.

Panteli, M., Pountos, I., Jones, E., and Giannoudis, P.V. (2015). Biological and molecular profile of fracture non-union tissue: current insights. J. Cell. Mol. Med. *19*, 685-713.

Ray, S.K., Li, H.J., Metzger, E., Schule, R., and Leiter, A.B. (2014). CtBP and associated LSD1 are required for transcriptional activation by NeuroD1 in gastrointestinal endocrine cells. Mol. Cell. Biol. *34*, 2308-2317.

Straza, M.W., Paliwal, S., Kovi, R.C., Rajeshkumar, B., Trenh, P., Parker, D., Whalen, G.F., Lyle, S., Schiffer, C.A., and Grossman, S.R. (2010). Therapeutic targeting of C-terminal binding protein in human cancer. Cell Cycle *9*, 3740-3750.

Wen, X., Chen, X., Liang, X., Zhao, H., Li, Y., Sun, X., and Lu, J. (2018). The small molecule NSM00191 specifically represses the TNF-alpha/NF-small ka, CyrillicB axis in foot and ankle rheumatoid arthritis. Int. J. Biol. Sci. *14*, 1732-1744.

Zhang, Q., Yao, H., Vo, N., and Goodman, R.H. (2000). Acetylation of adenovirus E1A regulates binding of the transcriptional corepressor CtBP. Proc. Natl. Acad. Sci. U. S. A. *97*, 14323-14328.

Zhang, W., Duan, N., Zhang, Q., Song, T., Li, Z., Chen, X., and Wang, K. (2018). The intracellular NADH level regulates atrophic nonunion pathogenesis through the CtBP2-p300-Runx2 transcriptional complex. Int. J. Biol. Sci. *14*, 2023-2036.

Zhao, L.J., Subramanian, T., and Chinnadurai, G. (2008). Inhibition of transcriptional activation and cell proliferation activities of adenovirus E1A by the unique N-terminal domain of CtBP2. Oncogene *27*, 5214-5222.